Peierls Transitions in Ionic Organic Charge-Transfer Crystals with Spin and Charge Degrees of Freedom†

S. A. Bewick and Z. G. Soos*

Department of Chemistry, Princeton University, Princeton, New Jersey 08544

Received: September 14, 2005; In Final Form: December 12, 2005

The quasi-one-dimensional electronic structure of organic charge-transfer (CT) salts rationalizes Peierls transitions in mixed or segregated stacks of π-electron donors (D) and acceptors (A). A microscopic Peierls−Hubbard model, H_{CT}, is presented for CT salts with mixed stacks $(D^{\rho+}A^{\rho-})_n$ and ionicity $\rho > 0.7$. Dimerization opens a Peierls gap that, due to electron correlation, is the singlet−triplet gap, E_{ST}. In contrast to spin-Peierls systems, such as Heisenberg spin chains with $\rho = 1$ and $T_{SP} < 20$ K, Peierls transitions in CT salts with $\rho < 1$ occur at higher T_P and involve both spin and charge degrees of freedom. Linear electron−phonon coupling and an adiabatic approximation for a harmonic lattice are used to model the dimerization amplitude $\delta(T)$ for $T < T_P$, the magnetic (spin) susceptibility $\chi(T)$, and the relative infrared intensity of totally symmetric molecular modes. Exact thermodynamics of H_{CT} for stacks up to $N = 12$ sites are applied to two CT salts with $T_P \sim 50$ and 120 K whose magnetism and infrared have not been modeled previously and to CT salts with inaccessibly high $T_P > 350$ K whose description has been difficult. Ionic CT salts are correlated Peierls systems with a degenerate ground state (GS) at $T = 0$ whose elementary excitations are spin solitons, while dimerized ion-radical stacks that support triplet-spin excitons have nondegenerate GS. In less ionic CT salts, modulation of H_{CT} parameters on cooling or under pressure leads to Peierls and/or neutral−ionic transitions of the GS, without appreciable thermal population of excited states. Correlations change the gap equation that relates E_{ST} at $T = 0$ to T_P compared to free electrons, and size convergence is fast in stacks with large $\delta(0)$ and high T_P.

1. Introduction

Peierls pointed out the instability of one-dimensional (1D) metals to distortions that open a gap at the Fermi energy.[1] In the half-filled case, the valence band is lowered and the conduction band is raised on dimerization to a state with alternating bond lengths $R = a \pm u$. The Su−Schrieffer−Heeger (SSH) model[2] of *trans*-polyacetylene, $(CH)_x$, contains the basic ingredients of a Peierls system: a 1D Hückel band of width $W = 4t$, linear electron−phonon (e-ph) coupling $\alpha = (dt/dR)_a$ and an adiabatic approximation for a harmonic lattice with force constant K. Thermal population of the conduction band at finite T reduces the energy gain on dimerization and the regular chain with $u = 0$ is regained at the Peierls temperature, T_P, where the system becomes metallic. Although $(CH)_x$ decomposes below T_P, it is a Peierls system with topological solitons above a degenerate dimerized ground state. Direct observation of Peierls transitions requires systems with narrow 1D bands in which electron−electron (e−e) correlations are likely to be important, as illustrated by Hubbard models with on-site repulsion $U > 0$.

Large $U > 4t$ in half-filled Hubbard or quantum cell models leads to Mott insulators with one electron per site in the ground state. Low-energy spin excitations are then governed by the kinetic exchange $J = 2t^2/U$ in a 1D Heisenberg antiferromagnet. Spin degrees of freedom and linear e-ph coupling $(dJ/dR)_a$ drive a spin-Peierls transition at T_{SP}. The lower energy scale makes spin-Peierls transitions accessible in either organic or inorganic linear chains. Bray et al.[3] have reviewed spin-Peierls transitions in organic systems with $T_{SP} < 20$ K, paying special attention to TTF^+ stacks (TTF = tetrathiafulvalene) in two systems with $T_{SP} = 12$ and 2.1 K, respectively; Cu^{2+} chains in $CuGeO_3$ with $T_{SP} = 14.5$ K have been analyzed by similar techniques.[4] Bray et al.[3] noted that since J is typically less than 300 K and T_{SP} cannot exceed $J/10$, systems that dimerize at $T > 50$ K have "generalized" Peierls transitions that involve both spin and charge degrees of freedom, but they did not treat such systems.

In this paper we consider generalized Peierls transitions in ionic organic charge-transfer (CT) salts that have not been modeled previously. Most theoretical studies of Peierls, spin-Peierls, and related transitions have focused on symmetry breaking or the $T = 0$ phase diagram of Hubbard and related models.[5−7] The ground state (GS) changes abruptly at critical values of model parameters, as we also find. We model instead the magnetic (spin) susceptibility that requires the full spectrum of excited states and vibrational intensities that rely on the recent Berry-phase formulation[8] of polarization. These quantities allow direct comparison with experiment. We further distinguish between Peierls and other mechanisms for dimerization in organic ion-radical salts.

CT salts are 1D insulators with mixed stacks[9] as sketched in Figure 1. There is π-overlap between donors (D) with low ionization potential I_D and acceptors (A) with high electron affinity A_A. Complexes of weak donors and acceptors have neutral GS with CT of $\rho < 0.3$ from D to A, while strong donors and acceptors have ionic GS with $\rho > 0.5$. At ionicity approaching $\rho = 1$, the 1D stack of D^+ and A^- ion radicals has spin degrees of freedom with exchange $J \sim t^2/\Delta E_{CT}$ for virtual transfers at the optical energy, $\Delta E_{CT} \sim 1$ eV. Suitable choices of D and A yield crystals with phase transitions on cooling or

† Part of the special issue "Robert J. Silbey Festschrift".

10.1021/jp0552022 CCC: $33.50
Published on Web 01/28/2006

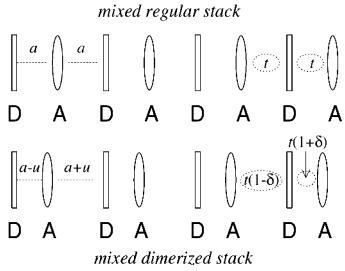

Figure 1. Schematic representation of mixed regular and dimerized stacks, with spacing a, $a \pm$ u and transfer integrals t, $t(1 \pm \delta)$.

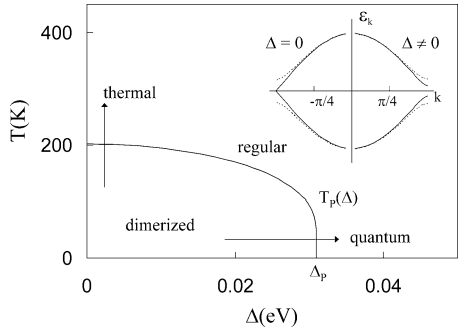

Figure 2. Peierls temperature T_P (Δ) in half-filled Hückel bands with site energies $\pm\Delta$. The inset shows reduced stabilization in insulators ($\Delta \neq 0$) compared to the metal ($\Delta = 0$). The GS is not dimerized for $\Delta^2 > \Delta_P^2$, a critical value that depends on lattice stiffness. The $T_P(\Delta)$ curve is based on $t = 0.17$ eV and $\epsilon_d = 0.28$ in eq 6.

under pressure.[10] The CT salts modeled in section 3 have constant $\rho \sim 0.9$. They are TTF−BA with[11] $T_P \sim 50$ K, M_2P-TCNQF$_4$ with[12,13] $T_P \sim 120$ K, and TMPD-TCNQ with[14] $T_P >$ 350 K, the limit of its thermal stability. Their Peierls transitions are from a regular ($u = 0$) insulating GS at high T, as known from their crystal structures, to a degenerate dimerized ($u > 0$) insulating GS, as inferred from magnetic and vibrational data.

A dimerized GS with spacing $a \pm u$ leads to transfer integrals $t(1 \pm \delta)$ along the stack and dimerization amplitude $\delta = \alpha u/t$ for linear e-ph coupling. Rice,[15] Pecile,[16] Girlando,[17] and co-workers have emphasized the dramatic spectroscopic consequences of breaking inversion symmetry. The Raman active totally symmetric (ts) molecular modes of the regular ($\delta = 0$) stack become IR active on dimerization, with polarization along the stack and huge intensity borrowed from the optical CT transition. The IR intensity of ts molecular modes provides a convenient and sensitive experimental probe of dimerization that directly implicates the charge degrees of freedom. We extend the Berry-phase formulation of polarization to excited states of insulators, thereby obtaining relative IR intensities as a function of $\delta(T)$.

The main features of mixed stacking are evident in a half-filled Hückel band with site energies $\pm\Delta$. Rice and Mele[18] generalized the SSH model to $\Delta > 0$. The $T_P(\Delta)$ curve in Figure 2 has maximum at $\Delta = 0$, the SSH case of a metal−insulator transition, and describes an insulator−insulator transition for $\Delta > 0$. Since the energy gain on dimerization decreases with Δ, as seen in the inset, the GS of a mixed stack with force constant K is not dimerized when Δ exceeds a critical $\Delta_P(K)$; the Peierls instability is conditional for $\Delta \neq 0$. Correlated models are necessary to have localized spins in 1D stacks. The qualitative new aspect of correlated models is a vanishing magnetic gap over an entire range of site energies rather than at a single point $\Delta = 0$. Accordingly, the Peierls instability is conditional on one side and unconditional on the other side of a critical value Γ_c; Γ_c is an electronic instability of rigid stacks, while the Peierls transition at $\Gamma_P > \Gamma_c$ is a structural instability of deformable stacks.

Most attention to the physics of CT salts has focused on neutral−ionic transitions or crossovers. The prototypical system[19−23] is TTF−CA, with CA = chloranil and $T_c = 81$ K at 1 atm. TTF−CA and related CT salts have increasing ρ on cooling or under pressure as the GS evolves from neutral and regular to ionic and dimerized. Horiuchi et al.[24] reported a quantum phase transition in DMTTF−BA (dimethyl-TTF, BA = bromanil) at 5 K as a function of applied pressure. In addition to structural and vibrational changes, the transition is marked by a large peak in the dielectric constant, a feature shared by several other CT salts[25] on cooling at ambient pressure. We have recently described[26] such dielectric peaks using the GS of a Peierls−Hubbard model, thereby treating them as quantum transitions. In terms of free electrons and Figure 2, modulation of Δ through Δ_P induces a quantum Peierls transition at $T \sim 0$ in systems with $k_BT \ll \Delta$. A thermal Peierls transition, by contrast, occurs at constant Δ in systems with low-energy excitations.

The microscopic Peierls−Hubbard model of CT salts in section 2 follows the SSH model with linear e-ph coupling and an adiabatic approximation for a harmonic lattice. In addition, it contains site energies that modulate ρ, the degree of CT, and strong e−e correlations that exclude D^{2+} and A^{2-} sites on physical grounds. Instead of approximations for extended systems, we solve the electronic problem exactly for finite stacks. The dimension of the basis is intermediate between the Hubbard and spin-only basis. Variable ρ makes it possible to model contributions from charge degrees of freedom. Rigid DA stacks with $\rho < \rho_c$ are diamagnetic band insulators with a finite band gap, while rigid D^+A^- stacks with $\rho > \rho_c$ are paramagnetic Mott insulators with a vanishing gap for spin excitations.[27]

Electron paramagnetic resonance (EPR) spectra[28] provided the first evidence for dimerization in anion radical stacks[29] of $TCNQ^-$ (TCNQ = tetracyanoquinodimethan) or cation radical stacks[30] of D^+; transitions in alkali-TCNQ almost reach[31] 400 K. Resolved fine structure, narrow EPR lines, and finite magnetic gaps at low T indicate mobile triplet spin excitons (TSE) with parallel spins on adjacent sites[9] that mimic bound electron−hole pairs in singlet or triplet excitons. The distinctly different EPR spectra of ionic CT salts were understood in terms of mobile $s = 1/2$ spins that move independently.[32] With the insight gained from the SSH analysis,[2] which showed that excitations of Peierls systems relax into charged or neutral solitons, we infer that ionic CT salts are Peierls systems while other mechanisms drive dimerization in TSE systems. Such discrimination follows naturally from a microscopic model of generalized Peierls systems.

The paper is organized as follows. Section 2 summarizes the Peierls−Hubbard model for CT salts, H_{CT}, with three states per site and relates it to other models. The thermodynamics of H_{CT} are discussed with respect to finite-size convergence, the dimerization amplitude, the spin susceptibility, and the IR intensity. Section 3 contains exact results for $(DA)_n$ oligomers up to $n = 6$ and applications to TTF−BA, M_2P-TCNQF$_4$, and TMPD-TCNQ. Section 4 addresses the relation between T_P and the magnetic gap at $T = 0$ in these correlated 1D stacks and summarizes evidence for spin solitons in ionic CT salts.

2. Peierls−Hubbard Model for CT Salts

There is a simple physical basis for neutral or ionic CT salts.[28] Consider a neutral crystal of N donors and N acceptors: The energy to transfer N electrons from D to A in the ionic lattice

is $N(I_D - A_A - M)$, where I_D is the ionization potential of D, A_A is the electron affinity of A, and M is the electrostatic (Madelung) energy per unit cell. The parameter $2\Gamma = I_D - A_A - M$ is used below for mixed stacks. Weak donors and acceptors have $\Gamma > 0$ and a neutral GS with $\rho = 0$ in the limit of no overlap; strong D and A have $\Gamma < 0$ and an ionic GS with $\rho = 1$ in this limit. The Mulliken CT integral $t(a \pm u) = -\langle D^+\alpha A^-\beta|H|DA\rangle$ mixes the electronic states of neighbors and depends on dimerization. Finite t generates $\rho > 0$ in neutral stacks and $\rho < 1$ in ionic stacks, while π-overlap in mixed stacks immediately rationalizes a 1D electronic structure and CT polarization along the stack.

We model the CT stacks in Figure 1 with electronic states D, $D^+\sigma$ and A, $A^-\sigma$, linear e-ph coupling $\alpha = (dt/dR)_a$, dimerization $\delta = \alpha u/t$, and inverse stiffness $\epsilon_d = \alpha^2/Kt$. The GS of a stack with a donor at $p = 1$ and an acceptor at $p = N$ is given by[33,34, 43]

$$H_{CT}(\Gamma,\delta) = \Gamma\sum_p(-1)^p n_p - t\sum_{p\sigma}[1 - \delta(-1)^p](a_{p\sigma}{}^+ a_{p+1\sigma} + hc) + N\delta^2/2\epsilon_d \quad (1)$$

with $t = 1$ as the unit of energy. The lattice treatment follows the SSH model.[2] The parameter $\Gamma = (I_D - A_A - M)/2$ describes D and A sites and incorporates 3D electrostatic interactions. In terms of a Hubbard model with $U > 0$ and site energies $\pm\Delta$ at A and D, respectively, we have $2\Gamma = 2\Delta - U$. The restriction $n_p = 1$ or 2 at D sites and 0 or 1 at A sites follows[35] in the limit Δ, $U \rightarrow \infty$ while keeping Γ finite. The restriction on n_p hardly matters for $\Gamma > t$, when the GS has paired electrons on D in a band insulator. The restriction is crucial for $\Gamma < -t$, when the GS has one electron on every site in a Mott insulator. H_{CT} smoothly connects band and Mott insulators. As discussed elsewhere,[9,34] Coulomb interactions within a stack can be added exactly to H_{CT}, but are typically treated in mean-field theory, while Coulomb interactions between stacks require mf analysis.

H_{CT} and related models conserve the total spin S. The GS is always a nondegenerate singlet, $S = 0$, even on adding arbitrary spin-independent intersite interactions to (1). Physically, $S = 0$ is stabilized the most by CT. The regular ($\delta = 0$) stack has a diamagnetic to paramagnetic transition[27] around $\Gamma_c \sim 0$ that marks the neutral−ionic crossover. Exact results[34] for H_{CT} at $\delta = 0$ up to $N = 22$ and 18 for $S = 0$ and 1, respectively, extrapolate to $\Gamma_c = -0.666t$ and $\rho_c = 0.684$ for the infinite stack. The lowest triplet or singlet excitation has vanishing energy for $\Gamma < \Gamma_c$ ($\rho > \rho_c$). The Peierls instability of H_{CT} defines a second critical value, Γ_P. A stack with $\epsilon_d > 0$ in (1) dimerizes at $\Gamma_P(\epsilon_d) > \Gamma_c$ given by

$$\frac{1}{\epsilon_d} = -\left(\frac{\partial^2\epsilon_0(\Gamma_P,\delta)}{\partial\delta^2}\right)_0 \quad (2)$$

Here $\epsilon_0 = E_0(\Gamma,\delta)/N$ is the absolute electronic energy per site in units of t, and the curvature of ϵ_0 diverges at $\delta = 0$ for all $\Gamma < \Gamma_c$. The inverse stiffness ϵ_d fixes Γ_P at $T = 0$ and the amplitude $\delta(\Gamma,0)$ for $\Gamma < \Gamma_P$. The Peierls transition at constant $\Gamma < \Gamma_P$ occurs at $T_P(\Gamma)$ where $\delta(\Gamma,T_P) = 0$.

We mention several limits of H_{CT}. First, for large δ we neglect the $(1 - \delta)$ terms in eq 1, thereby restricting CT to pairs of sites $2p - 1$, $2p$, and reducing the stack to two-electron systems. The dimer approximation to H_{CT} is not suitable for analysis of the Peierls transition that, by definition, requires knowledge of the GS at $\delta = 0$, but analytical and numerical results for dimers[36] have surprisingly great scope. Second, the limit $\Gamma \ll -t$ with $\rho = 1$ leads to spin chains with antiferromagnetic exchange.[9] Magnetic properties of H_{CT} at $\delta = 0$ are then given by the linear Heisenberg AF

$$H_{AF} = 2J\sum_p(\vec{s}_p\cdot\vec{s}_{p+1} - 1/4) \quad (3)$$

with $s_n = 1/2$ and $J = t^2/2|\Gamma|$. The $U \gg t$ limit of Hubbard models with equal site energies has $J = 2t^2/U$ and illustrates spin-charge separation. The physics is the same: virtual states with two electrons on the same site have energy U or $2|\Gamma|$, respectively, and H_{CT} has exactly half as many virtual excitations since transfer from D^+A^- is restricted to DA. Finally, the GS in the limit of $\Gamma \gg t$ has donors with $n_D \sim 2$ and acceptors with $n_A \sim 0$. The restrictions on n_p in eq 1 have practically no effect and H_{CT} reduces to the band limit.

A. Peierls Transition. We consider Peierls transitions in both H_{CT} and bands. The latter has no restrictions on n_p in (1) and can readily be solved for infinite stacks; we use $\pm\Delta$ rather than $\pm\Gamma$ for site energies. The filled valence band has energies $-\epsilon_k$ in the first Brillouin zone, with

$$\epsilon_k(\Delta,\delta) = \sqrt{\Delta^2 + 4\cos^2 k + 4\delta^2\sin^2 k} \quad (4)$$

Either Δ or δ leads to pairing of states k and $k + \pi$, as discussed[37] for spinless fermions in H_{AF}, and such pairing is closely related to the BCS treatment of superconductivity.[38,39] The GS dimerization $\delta = \delta(0)$ of the band is[18]

$$\frac{1}{\epsilon_d} = -\frac{1}{\delta}\left(\frac{\partial\epsilon_0(\Delta,\delta)}{\partial\delta}\right)_\delta = \frac{4[K(q) - E(q)]}{\pi q\sqrt{1-\delta^2}} \quad (5)$$

where E, K are complete elliptic integrals of the first and second kind with $q^2 = 4(1 - \delta^2)/(4 + \Delta^2)$ and $\Delta^2 < \Delta_P^2$. The temperature dependence of the Peierls gap is obtained[38,39] as in BCS

$$\frac{1}{\epsilon_d} = \frac{2}{\pi}\int_0^{\pi/2} 4\sin^2 k\, dk \frac{\tanh[\epsilon_k(\Delta,\delta)/2k_BT]}{\epsilon_k(\Delta,\delta)} \quad (6)$$

with $\delta = 0$ at $T_P(\Delta)$. The curve in Figure 2 is for $\epsilon_d = 0.28$ and $t = 0.17$ eV. The gap equation can be readily converted to an integral over $d\epsilon$ rather than dk. It differs from BCS in that the integral is over the entire band in Figure 2 rather than a narrow region about the Fermi energy. Peierls gaps of 10−20% of the bandwidth are found in polyacetylene or in ion-radical salts, and the dispersion relation (eq 4) must be retained. The BCS result of $E_g/T_P = 3.52$ is recovered at $\Delta = 0$ for $\delta(0) \ll 1$ and holds to within 5% up to $\delta(0) = 0.20$.

An adiabatic approximation for a harmonic lattice leads to a general relation between T_P and $\delta(0)$,

$$\frac{1}{\epsilon_d} = \frac{-1}{N\delta(0)}\left(\frac{\partial E_0}{\partial\delta}\right)_{\delta(0)} = \frac{-1}{N}\left\langle\left(\frac{\partial^2 E}{\partial\delta^2}\right)_0\right\rangle_{T_P} \quad (7)$$

The derivative of the GS energy per site of the dimerized stack is equal to the thermal average at T_P of the curvature per site of the $\delta = 0$ stack, as illustrated by eqs 5 and 6 in the band limit. Quite generally, increasing ϵ_d yields soft stacks with large $\delta(0)$ and high T_P. The second equality relates constant $\delta(0)$ to $T_P(N)$ in finite systems of equal size and variable $\epsilon_d(N)$. Substantial $\delta(0) > 0.05$ makes it possible to model extended stacks with

modest N. Much larger N is required for small gaps in BCS superconductors with $T_c \sim 10$ K that is less than 0.1% of $E_F \sim 2$ eV.

It is instructive to consider the two terms of eq 7 separately, the first as a function of δ at $T = 0$ and the second as a function of T at $\delta = 0$. The thermal average is over the energies of the $\delta = 0$ stack and diverges at $T = 0$ for $N \rightarrow \infty$. It is large but finite for $T > 0$, as seen in eq 6 where cos k in the denominator is canceled at $k \sim \pi/2$ by the tanh factor. The thermal average decreases with T and vanishes as $1/k_BT$ in the limit $T \rightarrow \infty$ when bonding and antibonding orbitals are equally populated. Thermal averages converge more rapidly with N at high T when many states are appreciably populated. It follows that the two terms in eq 7 are equal at some $T_P(N)$ that exceeds the minimum energy gap of the $\delta = 0$ stack.

Convergence can be followed for free electrons, whose gap equation (eq 6) is easily solved for finite $N = 4n + 2$. To simulate Peierls transitions in extended systems, finite-size gaps at $\delta = 0$ must clearly be comparable to or less than gaps induced by $\delta \sim 0.1$. For the band case, the Fermi wave vector for $N = 4n + 2$ in eq 4 is $k_F = \pi/2 - \pi/N$. The finite-size and dimerization contributions to the minimum gap are equal when $\epsilon_{k_F}(\Delta,\delta) = 2\epsilon_{k_F}(\Delta,0)$. It follows immediately from eq 4 that $\delta = 0.1$ requires $N \sim 50$ at $\Delta = 0$ and larger N for $\Delta > 0$. Direct evaluation of $T_P(\Delta)$ using a sum over k states in eq 6 confirms the convergence to the integral around $N \sim 50$. Fortunately, convergence is faster for H_{CT}. In the Heisenberg limit, E_{ST} is the lowest excitation energy. Exact results[40] up to $N = 20$ show that E_{ST} decreases as $1/N$ and that $E_{ST}(\delta) = 2E_{ST}(0)$ is achieved at $\delta = 0.02$ for $N = 14$. Direct solution of H_{CT} to $N = 14$ indicates that E_{ST} at $\delta \sim 0.1$ has a larger dimerization than finite-size contribution.

It remains to find the thermal average in eq 7 for H_{CT} with $\Gamma < \Gamma_c$. At constant Γ or volume, the Helmoltz free energy per site governs the thermodynamics. We define $\Delta_{nS}(\Gamma,\delta)$ as the excitation energy from the absolute GS, $E_0(\Gamma,\delta) = N\epsilon_0(\Gamma,\delta)$, to the nth energy in the manifold with $S = 0, 1, ..., N/2$. The partition function and free energy per site are

$$Q(\Gamma,\delta,T) = \sum_{S=0}^{N/2}(2S+1)Q_S = \sum_{S=0}^{N/2}(2S+1)\sum_n \exp(-\Delta_{nS}/k_BT) \tag{8}$$

$$A(\Gamma,\delta,T) = \epsilon_0(\Gamma,\delta) + \frac{\delta^2}{2\epsilon_d} - \frac{k_BT}{N}\ln Q(\Gamma,\delta,T) \tag{9}$$

The equilibrium dimerization is obtained by minimization of $A(\Gamma,\delta,T)$,

$$0 = \frac{\partial\epsilon_0}{\partial\delta} + \frac{\delta}{\epsilon_d} + \frac{1}{NQ}\sum_{S,n}(2S+1)\left(\frac{\partial\Delta_{nS}}{\partial\delta}\right)\exp(-\Delta_{nS}/k_BT) \tag{10}$$

At $T = 0$ the first two terms give $\delta(0)$. The last term is the thermal average per site of $\partial\Delta/\partial\delta$ at δ. We use $\delta(0)$ to eliminate ϵ_d and obtain a convenient expression for $\delta(T)/\delta(0)$,

$$\frac{\delta(T)}{\delta(0)}\left(\frac{\partial\epsilon_0}{\partial\delta}\right)_{\delta(0)} = \left(\frac{\partial\epsilon_0}{\partial\delta}\right)_{\delta(T)} + \frac{1}{N}\left\langle\left(\frac{\partial\Delta}{\partial\delta}\right)_{\delta(T)}\right\rangle_T \tag{11}$$

The thermal average is given in eq 10, with excitations Δ_{nS} evaluated at constant δ. We choose $\delta < \delta(0)$, find the energies and energy derivatives, and then solve eq 11 for T. We find T_P by taking $\delta = 0.001$ or by using eq 2 with the curvature of $A(\Gamma,0,T_P)$.

B. Spin Susceptibility and IR Intensity. Since H_{CT} conserves S, the spin susceptibility per site, $\chi(T)$, has Curie contributions from all thermally populated states,

$$\chi(T) = \frac{g^2{\mu_B}^2}{3k_BTNQ}\sum_{S=1}^{N/2}S(S+1)(2S+1)Q_S \tag{12}$$

Here μ_B is the Bohr magneton, Q_S is defined in eq 8, and g is close to the free value of 2.0023 in organic radicals, since light atoms have small spin−orbit coupling. The $\chi(T)$ results below are for finite stacks with variable Γ and δ. The Curie law for a spin with $s = 1/2$ is $\chi_C = g^2{\mu_B}^2/4k_BT$. The spin density $\rho_{sp}(T)$ has a central role in EPR studies[28,41] and is related[42] to spin correlation functions via the fluctuation−dissipation theorem,

$$\rho_{sp}(T) \equiv \frac{\chi(T)}{\chi_C(T)} = 1 + \sum_{n>1}4\langle\vec{s}_1\cdot\vec{s}_n\rangle_T/3 \tag{13}$$

where $\langle\cdots\rangle_T$ indicates a thermal average. AF correlations that decrease χ(T) at low T have long range, but the range decreases with T and vanishes as $T \rightarrow \infty$. Physically, ρ_{sp} is the fraction of spins seen in EPR or present at T_P. The lowest excitations are triplets with increased ρ compared to the GS. So $\rho(T) = \langle n_{2p}\rangle_T$ increases slightly with T at constant Γ, but the change is small and we use the GS value of ρ.

In contrast to the spin susceptibility, modeling the IR intensity of TS molecular modes requires recent theory.[26,43] The electronic polarization P per unit length and charge of an extended insulator is defined as a phase,[8]

$$P = \frac{1}{2\pi}\mathrm{Im}[\ln\langle G|\exp(2\pi iM/N)|G\rangle] \tag{14}$$

where $|G\rangle$ is the exact GS of the N-site system with periodic boundary conditions and $M = \Sigma_p r_p q_p$ is the dipole operator for charges q_p at r_p. We have $\langle q_p\rangle = \pm\rho$ at D and A sites, respectively, in the GS and take $r_p = pa$ along the stack for simplicity. $P(\Gamma,\delta{=}0)$ vanishes due to inversion symmetry at each site. Modulation of Γ by ts molecular modes induces electronic fluxes to neighbors that are precisely equal in $\delta = 0$ stacks.[43] There is a net flux on dimerization, however, when the ts modes become IR active with intensity proportional to $(\partial P/\partial\Gamma)^2$. CT salts are insulators with negligible thermal population of charge carriers under ambient conditions. The generalization of P in eq 14 to insulating states $|S,n\rangle$ with energy E_{Sn} is straightforward and yields contributions $(\partial P_{Sn}/\partial\Gamma)^2$ to the IR intensity. The intensity $I_{IR}(T)$ is the thermal average,

$$I_{IR}(\Gamma,\delta(T)) = C\langle(\partial P/\partial\Gamma)_{\delta(T)}{}^2\rangle_T \tag{15}$$

where C is a proportionality constant. Exact eigenstates of H_{CT} are used to compute P, P_{Sn}, and $I_{IR}(\Gamma,\delta)$ for finite N.

3. Results and Applications to CT Salts

As summarized in the Appendix, spin and spatial symmetries reduce eq 1 to a series of matrices, the largest of which is about 7000×7000 for $N = 12$. The eigenvalues $\epsilon_0(\Gamma,\delta)$ and $\Delta_{nS}(\Gamma,\delta)$ in subspaces with spin S give the partition function $Q(\Gamma,\delta,T)$ in eq 8. The matrices for $N = 10$ are about seven times smaller, while the Hubbard basis for $N = 12$ is more than 20 times larger and is far more demanding computationally. We start with the Peierls transition of H_{CT} at constant Γ and then model ionic CT salts with $T_P > 50$ K.

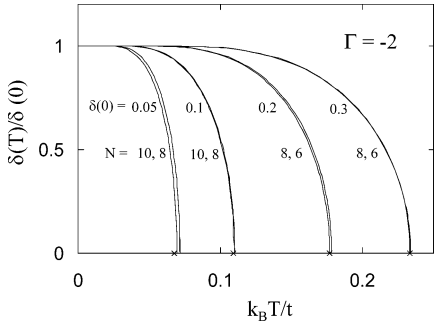

Figure 3. Temperature dependence of the dimerization amplitude, $\delta(T)$ in eq 10, of N-site stacks with $\Gamma = -2t$ ($\rho \sim 0.9$) and inverse stiffness ϵ_d in H_{CT} leading to $\delta(0)$ at $T = 0$. Crosses mark the Peierls temperature T_P of $N = 12$ stacks.

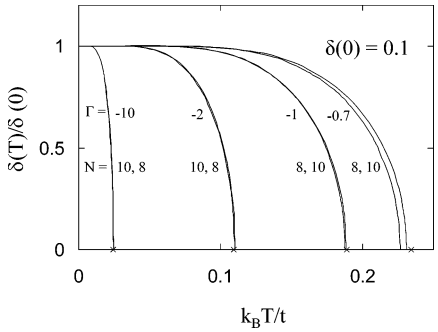

Figure 4. Temperature dependence of the dimerization amplitude, $\delta(T)$, of N-site stacks with the indicated Γ and ϵ_d in H_{CT} leading to $\delta(0) = 0.10$ at $T = 0$. Crosses mark the Peierls temperature T_P of $N = 12$ stacks. $T_P(N)$ decreases with N at $\Gamma = -10$ or -2 and increases with N at $\Gamma = -1$ or -0.7.

The dimerization amplitude, $\delta(T)$, is shown in Figure 3 for ionic stacks of $N = 8$ and 10 with $\Gamma = -2t$. In view of the limited knowledge of ϵ_d, we consider representative values of $\delta(0)$. This amounts to treating $\delta(0)$ as the input in eq 10 and solving for ϵ_d at $T = 0$. The crosses in Figure 3 mark T_P for $N = 12$. There is appreciable N dependence only at $\delta(0) = 0.05$, which is less than the estimated δ of CT salts. As expected, T_P increases in soft lattices with large GS dimerization. The behavior of $\delta(T)/\delta(0)$ follows from general considerations of double-well potentials[44] and is of the BCS form: $\delta(T)$ is constant at $\delta(0)$ up to $T_P/2$ and varies as $(1 - T/T_P)^{1/2}$ close to T_P.

Fixed $\delta(0)$ in eq 10 implies an inverse stiffness $\epsilon_d(N)$ that decreases with N, as noted above in connection with eq 7. Size effects cancel to some extent because the virtual singlet excitations that enter the GS derivative at $\delta > 0$ are the states whose population restores a regular stack at T_P. Other values of Γ yield similar $\delta(T)/\delta(0)$ curves, as illustrated in Figure 4 for $\delta(0) = 0.10$. The highest T_P is around Γ_c ($\rho_c = 0.684$) where E_{ST} is largest, while the $\Gamma = -10$ stack has a spin-Peierls transition governed by H_{AF}. Crosses again mark T_P for $N = 12$. For small $\Gamma = -1$ or -0.7 near symmetry crossovers,[34] periodic boundary conditions result in strong $N = 4n$, $4n + 2$ effects. Systematic trends in N are regained, as shown, with antiperiodic boundary conditions for $N = 10$ and periodic boundary conditions for $N = 8$ and 12. Note that T_P increases with N near Γ_c but decreases with N for $\Gamma < -2$.

Next we obtain singlet−triplet gaps at $T = 0$ as a function of δ. Figure 5 shows $E_{ST}(\Gamma,\delta)$ for $N = 10$ and 14, and convergence for $\delta > 0.2$. The extended stack has[34] $E_{ST}(\Gamma,0) = 0$ for $\Gamma < \Gamma_c = -0.666$ and $E_{ST} > 0$ for $\Gamma > \Gamma_c$. The sharply different behavior of E_{ST} at $\Gamma = 0.0$ and -0.7 is evident in Figure 5. We use the dimer approximation to find

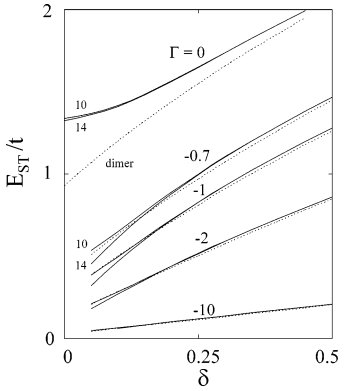

Figure 5. The energy gap E_{ST} from the ground state of H_{CT}, eq 1, to the lowest triplet as a function of dimerization δ for the indicated values of Γ and $N = 10$ and 14. Dashed lines are the dimer approximation in eq 16. The infinite $\delta = 0$ stack has $E_{ST} = 0$ for $\Gamma < \Gamma_c = -0.666$, finite E_{ST} for $\Gamma > \Gamma_c$.

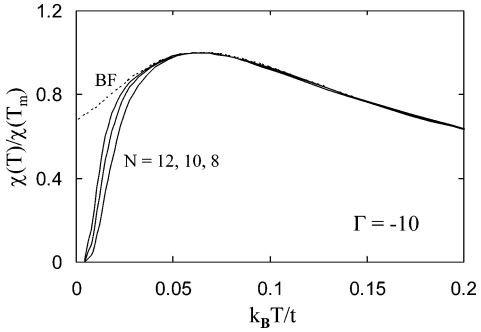

Figure 6. Magnetic susceptibility $\chi(T)$, eq 12, of N-site regular ($\delta = 0$) stacks with $\Gamma = -10t$ ($\rho > 0.99$) in H_{CT}, eq 1, normalized to the peak of the Bonner−Fisher (BF) susceptibility from ref 45 of H_{AF}, eq 3, with $J = t/20$. The dashed BF curve is a polynomial fit from ref 47. The exact value of $\chi_{BF}(0)$ is from ref 46.

E_{ST} to the second order in $(1 - \delta)$,

$$E^{(2)}_{ST,d} = (1 + \delta)\sqrt{2(1 - \rho_d)/\rho_d}(1 - {\rho_d}^2\nu^2(2 - 5\rho_d/2))$$

$$\rho_d = (1 - \Gamma/\sqrt{\Gamma^2 + 2(1 + \delta)^2})/2 \qquad (16)$$

and $\nu = (1 - \delta)/(1 + \delta)$. The dashed lines in Figure 5 are the dimer approximation (eq 16), which is adequate down to modest dimerization, but fails at $\delta = 0$, where the $\Gamma < \Gamma_c$ gap opens as $|\delta|$ while the finite gap for $\Gamma > \Gamma_c$ initially increases as δ^2. Nevertheless, eq 16 rationalizes how E_{ST} varies with ρ and δ. E_{ST} is the Peierls gap in ionic stacks with $\Gamma < \Gamma_c$ ($\rho > \rho_c$). Peierls transitions in less ionic systems do not open a gap, but merely increase it.

Figure 6 shows χ(T) for $\delta = 0$ stacks up to $N = 12$ with $\Gamma = -10$ in units of t, normalized to $\chi(T_m) = 1$ at the maximum. This is the ionic limit, with $\rho > 0.99$ and large energy of $20t$ for a DA pair, and serves as a numerical check by making contact with extensive results on the linear Heisenberg AF (eq 3). The Bonner−Fisher (BF) susceptibility,[45] $\chi_{BF}(T)$, is based on the exact[46] $\chi(0)$ and interpolation with numerical solutions of finite ($N < 12$) chains at finite T. The dashed line is a polynomial fit[47] to $\chi_{BF}(T)$ with $J = t^2/2|\Gamma| = t/20$ in eq 3. The $N = 8-12$ curves shown for the larger basis of H_{CT} properly reduce to BF results. As expected, finite-size gaps that decrease with N dominate at low T. The broad maximum is at $k_B T_m = 1.282J$.

Eggert et al.[48] have corrected the BF result near $T = 0$, where the slope of $d\chi/dT$ diverges and the linear interpolation in Figure

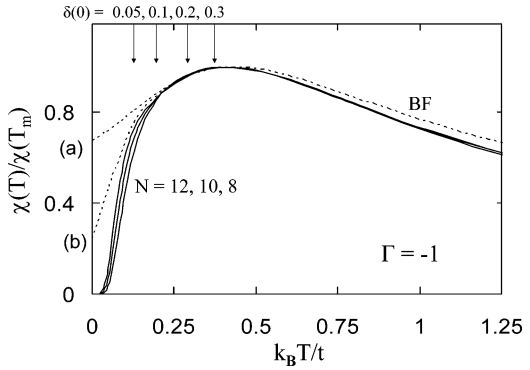

Figure 7. Magnetic susceptibility $\chi(T)$, eq 12, of N-site regular ($\delta = 0$) stacks with $\Gamma = -t$ ($\rho = 0.78$) in H_{CT}, eq 1, normalized to the peak $\chi_{BF}(T_m)$ of the dashed line, the susceptibility of H_{AF} with $J_{eff} = 0.66t^2 = 2|\Gamma|$. The $T \rightarrow 0$ extrapolation (a) is to $\chi_{BF}(0)$, while (b) contains a correction for H_{CT} described in the text. The arrows mark the Peierls temperature T_P of $N = 12$ stacks with GS dimerization $\delta(0)$ at $T = 0$.

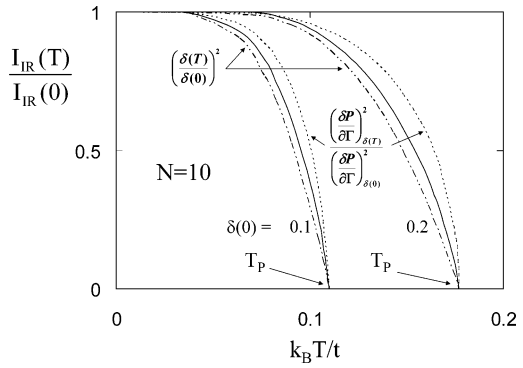

Figure 8. Relative IR intensity, eq 15, of a totally symmetric molecular vibration for $T < T_P$ in CT stacks with $N = 10$, $\Gamma = -2$ and dimerization $\delta(0) = 0.10$ and 0.20. Also shown are $[\delta(T)/\delta(0)]^2$ and the GS contribution, $[\partial P(\Gamma,\delta(T))/\partial\Gamma]^2$.

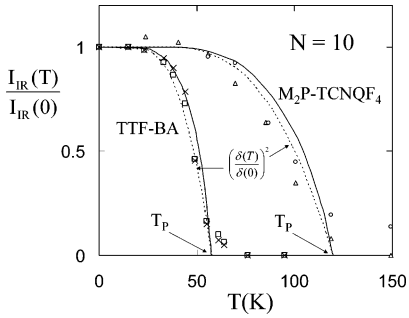

Figure 9. Relative IR intensity of TS molecular modes of TTF−BA and M_2P-$TCNQF_4$ for $T < T_P$. Solid lines are calculated using eq 15 for $N = 10$ and the model parameters in the text. The data for a TTF^+ and a BA^- vibration are from ref 11, while those for an M_2P^+ and $TCNQF_4^-$ vibration are from ref 13.

6 is too low for $k_BT < 0.1J$. This regime is suppressed by dimerization in Peierls systems. Johnston et al.[49] have extensively studied $s = 1/2$ chains with AF exchange and obtained $\chi(T)$ of the infinite chain to an accuracy of 4−5 significant places. Although a substantial advance over BF, such accuracy is beyond experimental comparison at present. Static susceptibility is always limited by diamagnetic corrections that must be estimated empirically, and often by small concentrations of paramagnetic impurities. The accuracy of integrating EPR lines limits direct measurement of the spin susceptibility. Hence the classic BF result suffices here.

Finite chains up to $N = 12$ yield $\chi(T)$ accurately for $T > T_m/4$ in Figure 6. The range of the spin correlation functions in eq 13 falls below N with increasing T. Since $\chi(0)$ is exact, the ratio $\chi(0)/\chi(T_m) = 0.676$ is quantitative, even though the BF interpolation is now known to fail. The exact $\chi(0)$ of H_{CT} is not known, but it is finite[34] in $\delta = 0$ stacks with $\Gamma < \Gamma_c$ and vanishes at Γ_c. Figure 7 shows $\chi(T)$ for $\delta = 0$ and $\Gamma = -1$, near Γ_c, with $\rho = 0.78$ and periodic boundary conditions for $N = 8$ and 12, antiperiodic boundary conditions for $N = 10$. Although no longer in the Heisenberg limit, the shape of $\chi(T)$ is similar and can be fit to an effective J_{eff} in H_{AF} that is reduced to $0.66\ t^2/2|\Gamma|$. The dashed line (a) is extrapolated to $\chi(0) = 0.676\chi(T_m)$. The line (b) contains the additional factor $(\rho - \rho_c)/(1 - \rho_c)$ that corrects for $\rho < 1$ and ensures $\chi(0) = 0$ at Γ_c where $\rho_c = 0.684$. We take line (b) for H_{CT} but note again that $T \sim 0$ and $\delta = 0$ does not occur in Peierls systems. Deviations from the Heisenberg limit are also evident in Figure 7 at high T where neutral excitations reduce $\chi(T)$.

The arrows in Figure 7 mark the Peierls transitions T_P for $N = 12$ based on eq 11 for $\delta(0) = 0.05$, 0.1, and 0.2; $N = 8$ or 10 suffices for $\delta > 0.10$. Convergence with N is naturally faster at large δ that localizes the GS and generates a large energy gap. We see that $N = 12$ is also sufficient at $\Gamma = -1$ and lower ρ for systems with $T_P/T_m > 1/4$. In the adiabatic approximation for the lattice, we obtain $\chi(T,\delta(T))$ with $\delta(T)$ variations shown in Figures 3 and 4. $\chi(T)$ curves of stacks with $\delta > 0$ resemble the $\delta = 0$ results in Figures 6 and 7, but are also accurate at low T when, for example, $N = 12$ is a good approximation for $E_{ST}(\Gamma,\delta)$.

The IR intensity (eq 15) of ts molecular modes of H_{CT} with $\Gamma = -2t$ and $\delta(0) = 0.10$ or 0.20 is shown in Figure 8. Excited states $|S,n\rangle$ are explicitly needed to evaluate P_{Sn}, but only a few contribute to the thermal average. For comparison, we also found the squared dimerization amplitude, $[\delta(T)/\delta(0)]^2$, and the normalized GS contribution, $[\partial P(\Gamma,\delta(T))/\partial\Gamma]^2$; they differ because $P(\Gamma,\delta)$ is already nonlinear in δ at $\delta = 0.1$. The thermal average $\langle(\partial P/\partial\Gamma)^2\rangle$ is reduced compared to the GS but exceeds $[\delta(T)/\delta(0)]^2$ slightly. As expected and emphasized in vibrational studies,[11,13,14] $I_{IR}(T)$ decreases with $\delta(T)$. In the dimer approximation, the intensity goes[17] as $\rho(1 - \rho)$ and is clearly related to charge fluctuations. Direct evaluation of $I_{IR}(T)$ and $\chi(T)$ affords a microscopic model of ionic CT salts with generalized Peierls transitions.

A. Ionic CT Salts with Peierls Transitions. TTF−BA has mixed regular stacks[11] at 300 K with ions at inversion centers. Vibrational data[11] indicate an ionic system with $\rho > 0.9$ (± 0.05) from 15 to 300 K, which sets $\Gamma = -2t$ ($\rho = 0.89$) in H_{CT}. Dimerization around $T_P \sim 50$ K is inferred[11] from both vibrational and magnetic data that we model with $t = 700$ K (0.060 eV) and $\delta(0) = 0.065$, which yields $T_P = 57$ K. The calculated IR intensity and absolute molar susceptibility are shown in Figures 9 and 10, respectively, as a function of T. The $\chi(T)$ curve is eq 12 with $g = 2.0023$ and $N = 12$ for $T > T_P$ and $N = 10$ for $T < T_P$. The $I_{IR}(T)$ curve is eq 15 with $N = 10$. The $I_{IR}(T)/I_{IR}(15\ K)$ data[11] are for the 944 cm^{-1} mode of BA^- (squares) and the 1423 cm^{-1} mode of TTF^+ (crosses). The $\chi(T)$ data have been corrected[11] for a diamagnetic contribution of 1.99×10^{-4} emu per mole and a Curie ($1/T$) contribution of 2.45% of $s = 1/2$ impurities.

The magnitude of $\chi(T)$ strongly constrains t. The shape of $\chi(T)$ depends somewhat on the treatment of the "impurity" spins whose precise behavior requires data to much lower T than 2 K. Curie tails that go as $1/T^\gamma$ power laws with $\gamma \sim 0.9$ are found in segregated $(TCNQ)_2^-$ stacks with disordered cations between the stacks.[50] Such a power law would reduce $\chi(T)$ by ∼10% around 100 K. For simplicity, we have neglected thermal

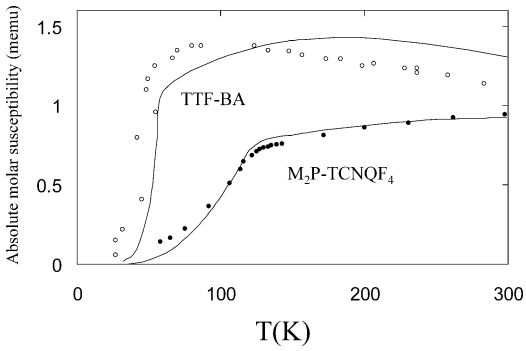

Figure 10. Temperature dependence of the absolute molar paramagnetic susceptibility of TTF−BA and M_2P-$TCNQF_4$. Solid lines are calculated using eq 12 with $N = 12$ for $T > T_P$, $N = 10$ for $T < T_P$, and the same model parameters as in Figure 9. The TTF−BA data is from ref 11, while the M_2P-$TCNQF_4$ data is from ref 12.

expansion and kept t constant from 15 to 300 K. Although approximate, the joint modeling of $\chi(T)$ and $I_{IR}(T)$ using H_{CT} is satisfactory.

M_2P-$TCNQF_4$ (M_2P = dimethylphenazine) has mixed regular stacks[12] at 300 K with ions at inversion centers. Vibrational data[13] down to 15 K indicates constant $\rho > 0.9$ (± 0.05) and dimerization below $T_P \sim 120$ K. The same interpretation[12] follows from $\chi(T)$, which goes as χ_{BF} with $J = 250$ K for $T > T_P$ and decreases rapidly at lower T on opening a gap. The ionicity fixes $\Gamma = -2t$ ($\rho = 0.89$) in H_{CT}. The absolute molar susceptibility in Figure 10 has $t = 1100$ K (0.095 eV), $\delta(0) = 0.09$ and $g = 2.0023$ in eq 12, again for $N = 12$ and 10 above and below T_P, respectively. The $\chi(T)$ data[12] were not corrected for a small Curie ($\sim 1/T$) contribution. The same parameters and $N = 10$ yield the normalized $I_{IR}(T)$ curve in Figure 9. The relative IR intensities[13] of an M_2P^+ mode (squares) and a $TCNQF_4^-$ mode (crosses) are normalized to 1.05. Good agreement in Figures 9 and 10 shows that H_{CT} accounts for this generalized Peierls transition with both charge and spin excitations. The spin density (eq 13) at T_P is $\rho_{sp} \sim 10\%$ in either TTF−BA or M_2P-$TCNQF_4$. There is considerable thermal population of triplets.

These initial fits of susceptibility and intensity data are preliminary in several ways. Explicit treatment of many (~ 10) coupled ts molecular modes with different linear e-ph coupling is used to analyze vibrational data.[16,17] The adiabatic approximation for the lattice is responsible for the sharp calculated transition at T_P. This approximation ignores fluctuations that suppress phase transitions in 1D systems. Even if electron transfer in CT salts is ideally 1D, the lattice and electrostatic energy are 3D. Explicit treatment of Coulomb interactions within and between stacks has to be compared with results based on $\Gamma = (I_D - A_A - M)/2$. Finally, we have neglected interactions between stacks that are known to be important from structural studies[22] of TTF−CA and related[51] CT salts. The low-T structure of M_2P-$TCNQF_4$ has not been reported, while that of TTF−BA has just appeared.[52]

We turn next to CT salts whose interpretation has been problematic. TMPD-TCNQ (TMPD = tetramethyl-*p*-phenylenediamine) has mixed regular stacks[53] at 300 K, albeit with unusually large thermal ellipsoids, and a transition around 220 K has been suggested.[54] A detailed vibrational study demonstrates[14] a dimerized GS at 15 K and $\rho \sim 0.93 \pm 0.05$ that increases from 0.88 ± 0.05 at 15 K to 0.97 ± 0.05 at 300 K. As shown in Figure 2 of ref 14, the relative IR intensities of several ts modes decrease by an order of magnitude, but are still finite at 350 K where the crystal decomposes. The observed behavior of $I_{IR}(T)/I_{IR}$ (15 K) resembles that shown in Figure 9 and extrapolates to zero at $T_P = 380 \pm 20$ K. The conflict between X-ray and vibrational data has been noted[14] but not resolved. As for the $\chi(T)$, it goes[55] as $T^{-1}\exp(-E_a/kT)$ with $E_a = 0.07$ eV (800 K) for $T > 160$ K, below which $s = 1/2$ impurities yield a Curie tail.

The vibrational data suggest a dimerized structure with a Peierls transition at $T_P = 380$ K, while $E_a = 800$ K indicates a GS with large $\delta(0)$. As expected from eq 7, a large Peierls gap and high T_P are related. We need larger $t \sim 0.2$ eV and $\delta(0) \geq 0.20$ to have $E_{ST} > E_a$. The calculated CT grows from $\rho = 0.87$ to $\langle \rho(T_P) \rangle = 0.92$ for $\Gamma = -2t$ and $\delta(0) = 0.20$. As shown by SSH for free electrons,[2] the elementary excitations of Peierls systems are topological solitons S or $S^{\pm}$ that connect regions of opposite dimerization; a pair of solitons has lower energy than the gap $E_g = 4t\delta$ between the valence and conduction bands. Since $E_{ST}(\Gamma,\delta)$ is the Peierls gap of H_{CT} for $\Gamma < \Gamma_c$, vertical excitation at E_{ST} is expected to relax into a pair of spin solitons[56] with $E_a < E_{ST}$ whose properties are sketched in the Discussion. First we comment on the magnitude of t and the implications of large $\delta(0)$ and high T_P.

Large $t \sim 0.22$ eV has been proposed[57,58] for TTF−CA and $t \sim 0.2$ eV (2300 K) is a typical estimate[9] for CT salts; hence the issue is small $t \sim 0.1$ eV in TTF−BA and M_2P-$TCNQF_4$. Direct quantum chemical calculation of t at $\pi-\pi$ separations of $R \sim 3.3$ Å is not yet possible to an accuracy of less than 0.1 eV. At the semiempirical level, t is proportional to the overlap integral $S(R)$ that can be evaluated reliably. The proportionality constant cancels for relative $t(R)$ values or for similar $\pi-\pi$ overlaps. Using crystal structures to evaluate $S(R)$ in several CT salts, we find[56] that t in TTF−CA or TMPD-TCNQ is more than twice as large as t in TTF−BA or M_2P-$TCNQF_4$, respectively. Larger t increases the energy gain on dimerization, and hence $\delta(0)$, provided that the inverse stiffness ϵ_d remains constant. We retain a harmonic lattice for simplicity but note that it may be inadequate at large $\delta(0)$.

Linear e-ph coupling leading to $(1 \pm \delta)$ in eq 1 is convenient mathematically, but restricted to small δ. An exponential dependence of $t(R)$ is expected on general grounds and leads to $\exp(\pm\delta)$ without changing $\alpha = (dt/dR)_a$. Dimerization then increases the average t as $\cosh \delta$. The simple unit cell of *trans*-$(CH)_x$ makes it possible to model its ts lattice modes at $\delta = 0$ that become IR active on dimerization in the presence of charged solitons. Quantitative analysis[59] of isotope effects and of photo or dopant-generated solitons decisively supports an exponential $t(R)$. Dimerization of $\delta(0) = 0.20$ increases the mean value of t by 2% without introducing any new parameters. It is customary to neglect, as we have in Figure 10, the temperature dependence of t or J in $\chi(T)$ fits, since it introduces a new parameter whose qualitative consequences are easily anticipated. Volume contraction on cooling or under pressure has a major role on the neutral−ionic transition of TTF−CA, however. The metal−insulator transition of TTF-TCNQ was intensively studied some years ago;[60] volume changes on cooling are known from structural studies[61] and transport data are fit with substantial ($\sim 10\%$) decrease[62] of t between 50 and 300 K. Constant t may be adequate when T_P is low, but perhaps not for $T_P \sim 380$ K.

To illustrate, we suppose that $t(T_P)$ is the constant t assumed so far. The motivation for this choice is to leave unchanged the immediate vicinity of the Peierls transition. Linear $t(T)$ increases $t(0)$ by a factor of $1 + \gamma$ that scales with T_P and could reach $\gamma \sim 10\%$ for $T_P \sim 400$ K. An exponential $t(R)$ gives another factor of $\cosh\delta(0)$ at $T = 0$. Increased dimerization $\delta'(0,\gamma) > \delta(0)$ at

$T = 0$ is given by eq 7 with

$$\epsilon'_d = \epsilon_d(1 + \gamma)\cosh\delta'(0,\gamma) \tag{17}$$

This equation is solved iteratively, starting with $\delta' = \delta(0)$. Since there is negligible thermal population of excited states for $T < T_P/2$, we need only GS properties to study $\gamma > 0$. We evaluate $(\partial P/\partial\Gamma)^2$ at $\delta'(0,\gamma) > \delta(0)$ to obtain the increased IR intensity at $T = 0$ due to thermal contraction and exponential $t(R)$ and find 13% higher intensity at $T = 0$ for $\delta(0) = 0.20$ and $\gamma = 10\%$. We solve eq 17 with $\gamma/2$ to obtain $\delta'(0,\gamma/2)$ at $T_P/2$ and the IR intensity due to the GS. Thermal expansion and exponential $t(R)$ confer some T dependence to the IR intensity for $T < T_P/2$ that is clearly found[14] in TMPD-TCNQ below 200 K. Such considerations must be taken into account in systems with high T_P and large $\delta(0)$. Until the TMPD-TCNQ parameters are better known, however, a more elaborate model is premature.

4. Discussion

The microscopic description of organic CT salts has been in terms of the Peierls−Hubbard model, H_{CT} in eq 1, for some time. The thermodynamics of H_{CT} obtained here account for Peierls transitions in systems with both spin and charge degrees of freedom. We have focused on magnetic and vibrational properties that, albeit for a simplified model, make contact with experimental data that have not been previously modeled. The susceptibility $\chi(T)$, vibrational data about ρ, and IR intensity of TS modes in TTF−BA and M_2P-TCNQF$_4$ are related to H_{CT} via Γ and ϵ_d, which yields the dimerization amplitude, $\delta(T)$. We found small $t \sim 0.10$ eV in these salts, less than the usual estimate for CT salts but consistent with overlap calculations.[56] Large bromine atoms significantly increase[11] the spacing a in Figure 1, thereby reducing t in TTF−BA. The spin density of the HOMO of M_2P^+ is concentrated on the central ring and so does not overlap well with the LUMO of TCNQ. Vibrational and magnetic data point to larger t and $\delta(0)$ in TMPD-TCNQ, whose inferred T_P is 380 K.

The Peierls gap of ionic CT salts is the singlet−triplet gap, $E_{ST}(\Gamma,\delta)$, that vanishes at $\delta = 0$ for $\Gamma < \Gamma_c$, where the Peierls instability of H_{CT} is unconditional. The relation between the dimerization amplitude, $\delta(0)$, and the transition temperature, T_P, is shown in Figure 11 for the wide parameter range of $0.05 < \delta(0) < 0.50$ and $-10 < \Gamma < -0.7$. The values of E_{ST} are for $N = 14$, while T_P values are for $N = 10$ and 12. The numerical results are well approximated by a straight line through the origin with slope $0.42 \sim 1/2.4$. The gap equation of H_{CT} is

$$E_{ST}(\Gamma,\delta(0)) = 2.4k_BT_P \tag{18}$$

Correlations associated with the exclusion of D^{2+} and A^{2-} sites yield a different gap equation than for free electrons, where $E_g = 3.52\ k_BT_P$ for $\delta(0) \ll 1$ and $\Delta = 0$ in eq 6. We are studying the gap equation in the Heisenberg limit and its convergence at larger N in order to treat phase transitions in correlated systems, as will be discussed elsewhere. We speculate that the same gap equation for systems with $1 > \rho > \rho_c = 0.684$ is due to the fact that E_{ST} is always the Peierls gap and that the lowest singlet excitation is at $2E_{ST}$. In the context of ionic CT salts, the experimental gap E_a is a lower bound on E_{ST} and hence on the model's T_P, but eq 18 is not used directly.

H_{CT} with constant Γ describes Peierls transitions driven by thermal populations. By contrast, TTF−CA and related salts with neutral−ionic transitions or crossovers have variable ρ that is modeled with variable Γ in H_{CT}. These salts are less ionic,

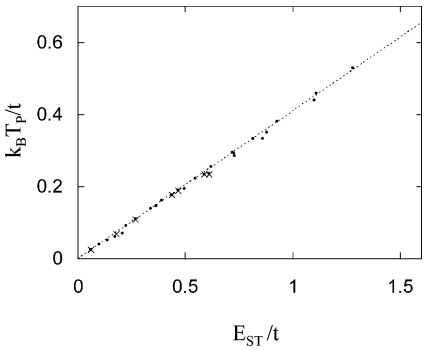

Figure 11. Peierls temperature T_P vs the singlet triplet gap E_{ST} at $T = 0$ of H_{CT} for Γ, $\delta(0)$ ranging from -10 to -0.7 and 0.05 to 0.50, respectively. $N = 14$ results are used for E_{ST} and $N = 10$ (dots) or 12 (crosses) for T_P. The dashed line through the origin has slope 0.42.

with $\rho < 0.7$ at low T and $\rho < 0.5$ for $T > 100$ K; accordingly, they have higher E_{ST} that has not been detected by EPR or susceptibility and negligible excited-state population. The distinction between systems with constant and variable ρ is qualitatively as follows. Cooling or pressure decreases the volume, which is the control parameter for GS transitions. Reduced volume increases the Madelung energy M, making $\Gamma = (I_D - A_A - M)/2$ more negative, and also increases t. Since CT mixing goes as t/Γ, this ratio increases strongly with decreasing volume in neutral systems with $\Gamma > 0$ and leads to variable ρ with $\rho \sim 0.5$ at $\Gamma \sim 0$. The situation is quite different in ionic lattices with $\Gamma < 0$ and $\rho > 1/2$ at ambient T and P. Decreasing volume now increases $|\Gamma|$ as well as t, so that CT mixing $t/|\Gamma|$ or ρ changes slowly. Since $I_D - A_A$ and M are typically far larger than k_BT at $T < 300$ K, variable ρ points to rare systems with finely balanced electronic interactions. Thermal Peierls systems are modeled in the present work.

We consider next another distinction, this one based on magnetic resonance (EPR), for which H_{CT} and the SSH model[2] offer a microscopic explanation. Conjugated polymers have wider bands ($4t \sim 10$ eV) and negligible populations of electronic excitations under ambient conditions. Optically generated singlet or triplet excitons in nondegenerate polymers relax due to e-ph coupling, but remain delocalized over a few unit cells. The unit cells of nondegenerate polymers are intrinsically large for chemical reasons. Peierls systems such as *trans*-$(CH)_x$ have a degenerate[2] GS and electronic excitations that relax into pairs of solitons that are free to move independently. The adiabatic approximation for a lattice with fixed $\delta(T)$ yields the Peierls transition at T_P that exceeds the thermal stability of $(CH)_x$. The same analysis for H_{CT} leads to a substantial spin density in eq 13, with $\rho_{sp} \sim 10\%$ at T_P for the two Peierls systems modeled in Figure 10. Much smaller $\rho_{sp} < 1\%$ is readily detectable in EPR at low temperature, when the lowest triplets are probed. Vertical excitations relax into spin solitons in Peierls systems with a degenerate GS, but form relaxed or adiabatic triplets in systems with nondegenerate GS.

Magnetic studies[28−30] of π-radical organic solids initially focused on triplet spin excitons (TSE) with $E_a \sim 0.1$ eV and narrow lines that indicate AF exchange interactions J and mobile spins. Soos and Bondeson[41] have summarized the magnetic properties of organic 1-D stacks. TSE are found in either segregated or mixed stacks. Resolved fine structure constants D and E are associated with magnetic dipolar interactions that decrease as R^{-3}, where R is the separation between the unpaired electrons. The unpaired electrons of TSEs move together and can be modeled by spins on adjacent radicals. Resolved fine structure is strong evidence that TSE systems are *not* Peierls

TABLE 1: Dimensions $W_N(S)$ of Subspaces with N Sited and Spin S in the Restricted Basis[a]

	$N = 8$	$N = 10$	$N = 12$
S	$W_8(S)$, $L_8(S)$	$W_{10}(S)$, $L_{10}(S)$	$W_{12}(S)$, $L_{12}(S)$
0	183, 109	1118, 607	7281, 3774
1	296, 161	2015, 1045	14 148, 7182
2	136, 75	1175, 610	9700, 4920
3	23, 14	310, 165	3389, 1730
4	1, 1	43, 20	603, 315
5		1, 1	47, 27
6			1, 1

[a] $L_N(S)$ is the dimension of the even subspace under $\sigma_b \times J$.

systems, as has been supposed[63] for alkali-TCNQ salts with phase transitions. It has long been known[31] that TSE systems with large E_a have small ρ_{sp} at the transition. Explicit modeling with H_{CT} is needed, however, to establish that ρ_{sp} is about 10% at the Peierls transition.

Qualitatively different EPR spectra, a single exchange-narrowed line, were observed in[55] TMPD-TCNQ, in[64,65] TMPD-CA, or in[66] PD-CA (PD = *p*-phenylenediamine). TMPD-CA has constant[67] $\rho \sim 0.65$ down to 15 K and regular stacks[68] at 300 K with large thermal ellipsoids. Its $E_a = 0.13$ eV (1500 K), as also found[66] in PD-CA, leads to high T_P according to eq 18. There are a few percent of $s = 1/2$ impurities in every case. In single crystals, the line widths indicate dipolar interactions[32,65] between independent $s = 1/2$ spins whose concentration increases as $\exp(-E_a/k_BT)$. The lowest excitation of a dimerized ionic stack is a pair of spin solitons that may schematically be represented as $(D^+A^-)_nD^+(A^-D^+)_n$ and $(A^-D^+)_nA^-(D^+A^-)_n$. Successive solitons are centered on D^+ and A^- along the stack. TMPD-TCNQ, TMPD-CA, and PD-CA are Peierls systems[56] with thermally accessible spin solitons and inaccessibly high T_P. Defect solitons have been identified[69] in TTF−CA at $T < T_c = 81$ K on the basis of resolved EPR signals whose intensity goes as $1/T$ and whose g-tensors correspond to TTF^+ and CA^-. We have recently discussed spin solitons[56] in ionic CT salts and emphasize here the qualitative difference between spin solitons and TSEs.

The thermodynamics of H_{CT} for finite N requires the eigenvalues of matrices whose dimensions are listed in Table 1 of the Appendix. We have suggested that good convergence with N is due to fairly large $\delta(0) > 0.05$ and correspondingly high T_P in eq 7. E_{ST} increases as $\delta(0)$ and a large gap localizes the GS. Localization due to Γ also aids convergence. We took advantage of the tremendous reduction of the basis on excluding D^{2+} and A^{2-} sites. The $N = 12$ thermodynamics of Hubbard models leads to matrices that are more than 20 times larger. The large Hubbard basis has recently been noted[70] in connection with partial spin-charge separation in TTF-TCNQ. Should the favorable size convergence of H_{CT} extend to Hubbard models, however, thermal Peierls transitions in Hubbard models of $N = 10$ or even 12 sites can be treated directly.

To summarize, there are two kinds of Peierls transitions in organic CT salts. In TTF−CA and related systems with variable ρ, H_{CT} describes[26] GS transitions that are driven by modulation of Γ and t on cooling or under pressure. In ionic salts with thermally accessible excited states, H_{CT} with constant Γ describes Peierls transitions in deformable stacks whose electronic structure differs from either the band or Heisenberg limits. The spin susceptibility and IR intensity of ts molecular modes are experimental probes of Peierls systems such as TTF−BA and M_2P-$TCNQF_4$ that have been modeled with H_{CT}. Ionic CT salts with high T_P are Peierls systems with spin solitons. The growing number of CT salts with a neutral−ionic or Peierls transitions[10] is another motivation for more flexible and general models. First-order transitions with discontinuous ρ require additions to H_{CT} in eq 1 such as mean-field Coulomb interactions or coupling to molecular vibrations.

Acknowledgment. Z.G.S. thanks A. Painelli, A. Girlando, and R.A. Pascal, Jr., for numerous discussions about CT salts and for valuable comments about this work.

Appendix

Since H_{CT} conserves the total spin S, we use a many-electron basis of valence bond (VB) diagrams $|k\rangle$ with fixed total spin S.[71] The spin basis for H_{AF} in eq 3 has 2^N spin states α or β with $n_p = 1$ for all p. The Hubbard basis has $n_p = 0$, 1, or 2 at each site and increases as 4^N for large N. The restricted basis without D^{2+} and A^{2-} sites increases as 3^N. Although $C_{N/2}$ symmetry leads to many-electron k-states, we have so far been unable to use translational symmetry except in the singlet subspace. Half-filled Hubbard models with nearest-neighbor t and equal site energies also have electron−hole symmetry[72] J that is lost in CT stacks. Reflection σ_b through the midpoint of any bond in Figure 1 interchanges the D and A sublattices. The combination $J \times \sigma_b$ is a symmetry operator for half-filled mixed dimerized stacks.[58] Since each diagram $|k\rangle$ has a unique partner $|k'\rangle = J \times \sigma_b|k\rangle$, even and odd linear combinations can be used to reduce subspaces with fixed S.

We define $(2S + 1)W_N(r,S)$ as the number of basis states with r cations D^+, r anions A^-, and total spin S in a stack of N molecules. The dimension of the restricted basis is the number of ways of distributing r ions, each with 2-fold spin degeneracy, on two sublattices. The total number of states is

$$W_N = \sum_{r=0}^{N/2}\sum_{S=0}^{r}(2S+1)W_N(r,S) = \sum_{r=0}^{N/2}2^{2r}\binom{N/2}{r}^2 \quad \text{(A.1)}$$

where $(\cdots)$ is the binomial coefficient, $2S + 1$ is the spin degeneracy in zero field, and r is the largest S for $2r$ ion radicals. We resolve 2^{2r} spin states into the number of representations, $W_N(r,S)$, with spin S

$$2^{2r} = \sum_{S=0}^{r}(2S+1)W_N(r,S) = \sum_{S=0}^{r}\frac{(2S+1)^2}{2r+1}\binom{2r+1}{r+1+S} \quad \text{(A.2)}$$

The decomposition is general. The dimensions of subspaces in the Heisenberg model are $W_N(N/2,S)$. Since finite t mixes states with different r but conserves S, we insert eq A.2 into eq A.1 and sum over r to obtain the dimensions $W_N(S)$ of subspaces with fixed S in the restricted basis. The same procedure holds for the Hubbard basis.

Table 1 lists the dimensions of exact subspaces, $W_N(S)$, in the restricted basis up to $N = 12$. Each $W_N(S)$ is resolved into two subspaces using $J \times \sigma_b$, and the dimension $L_N(S)$ of the larger one is given. H_{CT} is solved by diagonalizing matrices of dimensions $L_N(S)$ and $W_N(S) - L_N(S)$. The matrices are sparse but not symmetric because the VB basis is not orthogonal with respect to diagrams with identical charge distributions $\{n_p\}$ and different spin pairing of sites with $n_p = 1$. Increasing N by 2 increases the entries in Table 1 by a factor of roughly 7, which is less than the 9-fold increase at large N. The total number of states for $N = 12$ is $W_{12} = 127\,905$, well below $3^{12} = 531\,441$. For large N, the most probable value, $r_{mp} = N/3$, is found as usual from the largest term on the right in eq A.1 using Stirling's approximation for factorials. Hence the asymptotic value of W_N

is 3^N, as expected. The Hubbard basis has no restriction on n_p beyond charge conservation and has 2 704 156 states for $N = 12$, or about 16% of 4.[12]

References and Notes

(1) Peierls, R. E. *Quantum Theory of Solids*; Oxford: Clarendon, 1955; p 108.

(2) Su, W. P.; Schrieffer, J. R.; Heeger, A. J. *Phys. Rev. Lett.* **1979**, *44*, 1698. Su, W. P.; Schrieffer, J. R.; Heeger, A. J. *Phys. Rev. B* **1980**, *22*, 2099. Heeger, A. J.; Kivelson, S.; Schrieffer, J. R.; Su, W. P. *Rev. Mod. Phys*. **1988**, *60*, 81.

(3) Bray, J. W.; Interrante, L. V.; Jacobs, I. S.; Bonner, J. C. *Extended Linear Chain Compounds*; Miller, J. S., Ed.; Plenum: New York, 1983; Vol. 3; p 353.

(4) Hase, M.; Terasaki, I.; Uchinokura, K. *Phys. Rev. Lett*. **1993**, *70*, 3651.

(5) Lin, H. Q.; Campbell, D. K.; Clay, R. T. *Chinese J. Phys*. **2000**, *38*, 1. Kuprievich, V. A. *Phys. Rev. B* **1994**, *50*, 16872.

(6) Bohm, M. C. *Chem. Phys*. **1991**, *155*, 49. Lepine, Y.; Tannous, C.; Caille, A. *Phys. Rev. B* **1979**, *20*, 3753.

(7) Hellberg, C. S.; Mele, E. J. *Phys. Rev. Lett.* **1991**, *67*, 2080. Kobayashi, K.; Ohe, C.; Iguchi, K. *Phys. Rev. B* **1996**, *54*, 13129. Sirker, S.; Klumpfer, A. *Phys. Rev. B* **2002**, *66*, 245102.

(8) Resta, R. *Phys. Rev. Lett*. **1998**, *80*, 1800. Resta, R. *J. Phys: Condens. Matter* **2002**, *14*, R625 and references therein.

(9) Soos, Z. G.; Klein, D. J. *Treatise on Solid-State Chemistry*; Hannay, N. B., Ed.; Plenum: New York, 1976; Vol. III; p 689.

(10) Girlando, A.; Painelli, A.; Bewick, S. A.; Soos, Z. G. *Synth. Met*. **2004**, *141*, 129.

(11) Girlando, A.; Pecile, C.; Torrance, J. B. *Solid State Commun*. **1985**, *54*, 753.

(12) Soos, Z. G.; Keller, H. J.; Ludolf, K.; Queckbörner, J.; Nöthe, D.; Flandrois, S. *J. Chem. Phys.* **1981**, *74*, 5287.

(13) Meneghetti, M.; Girlando, A.; Pecile, C. *J. Chem. Phys*. **1985**, *83*, 3134.

(14) Girlando, A.; Painelli, A.; Pecile, C. *Mol. Cryst. Liq. Cryst*. **1984**, *112*, 325.

(15) Rice, M. J. *Solid State Commun.* **1979**, *31*, 93.

(16) Bozio, R.; Pecile, C. *Spectroscopy of Advanced Materials*, Adv. Spectrosc. Vol. 19; Clark, R. J. H., Hester, R. E., Eds.; Wiley: New York, 1991; p 1. Pecile, C.; Painelli, A.; Girlando, A. *Mol. Cryst. Liq. Cryst*. **1989**, *171*, 69.

(17) Painelli, A.; Girlando, A. *J. Chem. Phys*. **1985**, *84*, 5655.

(18) Rice, M. J.; Mele, E. J. *Phys. Rev. Lett*. **1982**, *49*, 1455.

(19) Torrance, J. B.; Vasquez, J. E.; Mayerle, J. J.; Lee, V. Y. *Phys. Rev. Lett*. **1981**, *46*, 253. Torrance, J. B.; Girlando, A.; Mayerle, J. J.; Crowley, J. I.; Lee, V. Y.; Batail, P.; LaPaca, S. J. *Phys. Rev. Lett*. **1981**, *47*, 1747.

(20) Girlando, A.; Marzola, F.; Pecile, C.; Torrance, J. B. *J. Chem. Phys*. **1983**, *79*, 1075.

(21) Takaoka, K.; Kaneko, Y.; Okamoto, H.; Tokura, Y.; Koda, T.; Mitani, T.; Saito, G. *Phys. Rev. B* **1987**, *36*, 3884.

(22) Le Cointe, M.; Lemee-Cailleau, M. H.; Cailleau, H.; Toudic, B.; Toupet, L.; Heeger, G.; Moussa, F.; Schweiss, P.; Kraft, K. H.; Karl, N. *Phys. Rev. B* **1995**, *51*, 3374.

(23) Luty, T.; Cailleau, H.; Koshihara, S.; Collet, E.; Takesada, M.; Lemée-Cailleau, M. H.; Buron-Le Cointe, M.; Nagaosa, N.; Tokura, Y.; Zienkiewicz, E.; Ouladdiaf, B. *Europhys. Lett.* **2002**, *59*, 619.

(24) Horiuchi, S.; Okimoto, Y.; Kumai, R.; Tokura, Y. *Science* **2003**, *299*, 229.

(25) Horiuchi, S.; Okimoto, Y.; Kumai, R.; Tokura, Y. *J. Am. Chem. Soc*. **2002**, *123*, 665.

(26) Soos, Z. G.; Bewick, S. A.; Peri, A.; Painelli, A. *J. Chem. Phys*. **2004**, *120*, 6712.

(27) Soos, Z. G.; Bondeson, S. R.; Mazumdar, S. *Chem. Phys. Lett*. **1979**, *65*, 331.

(28) Nordio, P. L.; Soos, Z. G.; McConnell, H. M. *Annu. Rev. Phys. Chem*. **1966**, *17*, 237.

(29) Chesnut, D. B.; Phillips, W. D. *J. Chem. Phys*. **1961**, *35*, 1002.

(30) Thomas, D. D.; Keller, H. J.; McConnell, H. M. *J. Chem. Phys*. **1963**, *39*, 2321.

(31) Vegter, J. G.; Himba, T.; Kommandeur, J. *Chem. Phys. Lett*. **1969**, *3*, 427.

(32) Soos, Z. G. *J. Chem. Phys*. **1967**, *46*, 4284.

(33) Strebel, P. J.; Soos, Z. G. *J. Chem. Phys*. **1970**, *53*, 4077.

(34) Anusooya-Pati, Y.; Soos, Z. G.; Painelli, A. *Phys. Rev. B* **2001**, *63*, 205118 and references therein.

(35) Soos, Z. G.; Mazumdar, S. *Phys. Rev. B* **1978**, *18*, 1881.

(36) Painelli, A.; Terenziani, F. *J. Phys. Chem. A* **2000**, *104*, 11041. Painelli, A.; Terenziani, F. *J. Am. Chem, Soc*. **2003**, *125*, 5624. Terenziani, F.; Painelli, A. *Phys. Rev. B* **2003**, *68*, 165405. Boldrini, B.; Cavalli, E.; Painelli, A.; Terenziani, F. *J. Phys. Chem. A* **2002**, *106*, 6286.

(37) Soos, Z. G. *J. Chem. Phys*. **1965**, *43*, 1121.

(38) Kittel, C. *Quantum Theory of Solids*; Wiley: New York, 1963; Ch. 8.

(39) Tinkham, M. *Low-Temperature Physics*; DeWitt, C., Dreyfus, B., DeGennes, P. G., Eds.; Gordon and Breach: New York, 1962; p 176.

(40) Soos, Z. G.; Kuwajima, S.; Mihalick, J. E. *Phys. Rev. B* **1985**, *32*, 3124.

(41) Soos, Z. G.; Bondeson, S. R. *Extended Linear Chain Compounds*; Miller, J. S., Ed.; Plenum: New York, 1983; Vol. 3, p 193.

(42) Soos, Z. G.; Cheung, T. T. P.; McGregor, K. T. *Chem. Phys. Lett*. **1977**, *46*, 600.

(43) Painelli, A.; Del Freo, L.; Soos, Z. G. *Synth. Met*. **2003**, *133*−*134*, 619. Del Freo, L.; Painelli, A.; Soos, Z. G. *Phys. Rev. Lett.* **2002**, *89*, 27402.

(44) Izyumov, Y. A.; Syromyatnikov, V. N. *Phase Transitions and Crystal Symmetry*; Kluwer Academic: Dordrecht, 1990; p 3.

(45) Bonner, J. C.; Fisher, M. E. *Phys. Rev.* **1964**, *135*, A640.

(46) Griffiths, R. B. *Phys. Rev.* **1963**, *133*, A768.

(47) Hatfield, W. E.; Estes, W. E.; Marsh, W. E.; Pickens, M. W.; ter Haar, L.; Weller, R. R. *Extended Linear Chain Compounds*; Miller, J. S., Ed.; Plenum: New York, 1983; Vol. 3, p 43.

(48) Eggert, S.; Affleck, I.; Takahashi, M. *Phys. Rev. Lett*. **1994**, *73*, 332.

(49) Johnston, D. C.; Kremer, R. K.; Troyer, M.; Wang, X.; Klumpfer, A.; Bud'ko, S. L.; Panchula, A. F.; Canfield, P. C. *Phys. Rev. B* **2000**, *61*, 9558.

(50) Bondeson, S. R.; Soos, Z. G. *Phys. Rev. B* **1980**, *22*, 1793.

(51) Collet, E.; Buron-Le Cointe, M.; Lemée-Cailleau, M. H.; Cailleau, H.; Toupet, L.; Meven, M.; Mattauch, S.; Heeger, G.; Karl, N. *Phys. Rev. B* **2001**, *63*, 054105.

(52) Garcia, P.; Dahaouie, S.; Fertey, P.; Wenger, E.; Lecomte, C. *Phys. Rev. B* **2005**, *72*, 104115.

(53) Hanson, A. W. *Acta Crystallogr*. **1965**, *19*, 619.

(54) Etemad, S.; Ehrenfreund, E. *AIP Conf. Proc*. **1972**, *10*, 1499. Sommano, R.; Hadek, V.; Yen, S. P. S.; Rembaum, A.; Deck, R. *J. Chem. Phys*. **1975**, *62*, 1061.

(55) Hoffman, B. M.; Hughes, R. C. *J. Chem. Phys*. **1970**, *52*, 4011.

(56) Bewick, S. A.; Soos, Z. G. *Chem. Phys*., in press.

(57) Painelli, A.; Girlando, A. *J. Chem. Phys*. **1987**, *87*, 1705.

(58) Soos, Z. G.; Kuwajima, S.; Harding, R. H. *J. Chem. Phys*. **1986**, *85*, 601.

(59) Soos, Z. G.; Mukhopadhyay, D.; Painelli, A.; Girlando, A. *Handbook of Conducting Polymers*, 2nd ed.; Skotheim, T. A., Elsenbaumer, R., Reynolds, J. R., Eds.; Marcel Dekker: New York, 1998; p 165.

(60) Keller, H. J., Ed. *Chemistry and Physics of One-Dimensional Metals*; NATO Adv. St. Inst. Series, B25; Plenum: New York, 1977. Kagoshima, S.; Nagasawa, H.; Samboni, T. *One-Dimensional Conductors*; Springer-Verlag: Berlin, 1988.

(61) Schultz, A. J.; Stucky, G. D.; Blessing, R. H.; Coppens, P. *J. Am. Chem. Soc*. **1976**, *98*, 3194.

(62) Conwell, E. M. *Phys. Rev. B* **1980**, *22*, 1761.

(63) Takaoka, Y.; Moizuku, K. *J. Phys. Soc. Jpn.* **1979**, *47*, 1752.

(64) Pott, G. T.; Kommandeur, J. *Mol. Phys.* **1967**, *13*, 373.

(65) Huang, T. Z.; Taylor, R. P.; Soos, Z. G. *Phys. Rev. Lett*. **1972**, *28*, 1054.

(66) Hughes, R. C.; Soos, Z. G. *J. Chem. Phys*. **1968**, *48*, 1066.

(67) Girlando, A.; Painelli, A.; Pecile, C. *J. Chem. Phys*. **1988**, *89*, 494.

(68) DeBoer, J. L.; Vos, A. *Acta Crystallogr. B* **1968**, *24*, 720.

(69) Mitani, T.; Saito, G.; Tokura, Y.; Koda, T. *Phys. Rev. Lett*. **1984**, *53*, 842.

(70) Claessen, R.; Sing, M.; Schwingenschlogl, U.; Carmelo, J. M. P. *J. Phys. IV France* **2004**, *114*, 51.

(71) Soos, Z. G.; Ramasesha, S. *Valence Bond Theory and Chemical Structure*; Klein, D. J., Trinajstic, N., Eds.; Elsevier: Amsterdam, 1989; p 81. Ramasesha, S.; Soos, Z. G *Theoretical and Computational Chemistry*; Cooper, D. L., Ed.; Elsevier: Amsterdam, 2002; Vol. 10, p 635.

(72) Bondeson, S. R.; Soos, Z. G. *J. Chem. Phys*. **1979**, *71*, 3807.